Supporting information for

s-Block Metal Ions Induce Structural Transformation Between Figure-Eight and Double Trefoil Knot

Li-Long Dang,[a] Xiang Gao,[a] Yue-Jian Lin,[a] and Guo-Xin Jin*[a]

Shanghai Key Laboratory of Molecular Catalysis and Innovative Materials, State Key Laboratory of Molecular Engineering of Polymers, Department of Chemistry, Fudan University, Shanghai 200438, P. R. China.

*E-mail: gxjin@fudan.edu.cn.

Contents

1. General considerations **2**

2. Synthesis of complexes 1, 2, 3 and 4 **3**

3. Single-crystal X-ray structure of figure-eight knot, 1, 2, 3a and 4 **6**

4. NMR spectra **18**

5. ESI-MS spectra **21**

6. DFT computational details **22**

7. X-ray crystallography details **28**

8. References **29**

1. General considerations

All reagents and solvents were purchased from commercial sources and used as supplied unless otherwise mentioned. The starting materials $[Cp^*RhCl_2]_2$ and ($Cp^*=\eta^5$-pentamethylcyclopentadienyl) [1], BiBzIm (BiBzIm = 2, 2′-bisbenzimidazole) [2] and ligand **L** were prepared by literature methods [3]. NMR spectra were recorded on Bruker AVANCE I 400 spectrometers at room temperature and referenced to the residual protonated solvent. Proton chemical shifts are reported relative to the solvent residual peak (δ H = 3.31 for CD_3OD). Coupling constants are expressed in Hertz.Elemental analyses were performed on an Elementar Vario EL III analyzer. IR spectra of the solid samples (KBr tablets) in the range 400–4000 cm^{-1} were recorded on a Nicolet AVATAR-360IR spectrometer. ESI-MS spectra were recorded on a Micro TOF II mass spectrometer.

2. Synthesis of complexes 1 2, 3 and 4

Synthesis of 1 (**Double trefoil knot**). $AgSO_3CF_3$ (62 mg, 0.24 mmol) was added to a solution of $[Cp^*RhCl_2]_2$ (37.2 mg, 0.06 mmol) in CH_3OH (6 mL) at room temperature. The reaction mixture was stirred in the dark for 24 h and then filtered. **BiBzIm** (14.04 mg, 0.06 mmol) was added to the filtrate. The mixture was stirred at room temperature for 12 h to give a yellow solution. **L** (20.76 mg, 0.06 mmol) and excess potassium nitrate (6.07 mg, 0.06mmol) was then added. The mixture was stirred at room temperature for another 12 h to give a yellow solution. The solvent was concentrated to about 3 mL. Upon the addition of diethyl ether, a yellow solid was precipitated and collected. The product was recrystallized from a CH_3OH/diethyl ether mixture to afford block-shaped crystals (**1**).

Characterization data for 1: 73.90 mg, yield 86.4%. ^1H NMR (400 MHz, CD_3OD, ppm, with respect to Cp*Rh): δ 8.58 (d, *J* = 6.0 Hz, 12H, pyridyl-αH), δ 7.13 (d, *J* = 5.6 Hz, 12H, pyridyl-αH), δ 8.15-8.11 (m, 12H, BiBzIm-H), δ 7.54-7.47 (m, 12H, BiBzIm-H), δ = 3.64 (d, *J* = 14.8 Hz, 6H, phenyl-H), δ = 1.66 (d, *J* = 16 Hz, 6H, phenyl-H), δ = 1.73 (s, 90H, Cp*-H). IR (KBr disk, cm^{-1}): v = 1709, 1671, 1617, 1534, 1454, 1417, 1373, 1333, 1271, 1224, 1143, 1067, 1031, 1003, 963, 771, 638, 572, 445. Anal. Calcd for $C_{340}H_{344}O_{56}N_{48}S_{14}F_{42}K_2Rh_{12}$ (M = 8552.89): C, 47.72; H, 4.05; N, 7.86. Found: C, 47.74; H, 4.02, N, 7.90. ESI-MS: m/z 2680.66 (calcd for $[M - 2CH_3OH - 3OTf^-]^{3+}$ 2680.66).

Synthesis of 2 (**Trefoil knot**). $AgSO_3CF_3$ (62 mg, 0.24 mmol) was added to a solution of $[Cp^*RhCl_2]_2$ (37.2 mg, 0.06 mmol) in CH_3OH (6 mL) at room temperature. The reaction mixture was stirred in the dark for 24 h and then filtered. **BiBzIm** (14.04 mg, 0.06 mmol) was added to the filtrate. The mixture was stirred at room temperature for 12 h to give a yellow solution. **L** (20.76 mg, 0.06 mmol) and excess calcium nitrate tetrahydrate (14.17 mg, 0.06mmol) was then added. The mixture was stirred at room temperature for another 12 h to give a yellow solution. The solvent was concentrated to about 3 mL. Upon the addition of diethyl ether, a yellow solid was precipitated and collected. The product was recrystallized from a CH_3OH/diethyl ether mixture to afford block-shaped crystals (**2**).

Characterization data for 2: 76.73 mg, yield 87.3%. ^1H NMR (400 MHz, CD_3OD, ppm, with respect to Cp*Rh): δ 8.60 (d, *J* = 5.6 Hz, 12H, pyridyl-αH), δ 7.14 (d, *J* = 5.6 Hz, 12H, pyridyl-αH), δ 8.14-8.12 (m, 12H, BiBzIm-H), δ 7.55-7.48 (m, 12H, BiBzIm-H), δ 3.58 (d, *J* = 14.4 Hz, 6H, phenyl-H), δ 1.67 (d, *J* = 15.2 Hz, 6H, phenyl-H), δ 1.73 (s, 90H, Cp*-H). IR (KBr disk, cm^{-1}): v = 1709, 1671, 1617, 1534, 1454, 1417, 1373, 1333, 1271, 1224, 1143, 1067, 1031, 1003, 963, 771, 638, 572, 445. Anal. Calcd for $C_{170}H_{168}O_{30}N_{24}S_8F_{24}CaRh_6$ (M = 4394.37): C, 46.43; H, 3.85; N, 7.64. Found: C, 46.41; H, 3.83, N, 7.61. ESI-MS: m/z 2048.23 (calcd for $[M - 2OTf^-]^{2+}$ 2048.23).

Synthesis of 3 (**Trefoil knot**). $AgSO_3CF_3$ (62 mg, 0.24 mmol) was added to a solution of $[Cp^*RhCl_2]_2$ (37.2 mg, 0.06 mmol) in CH_3OH (6 mL) at room temperature. The reaction mixture was stirred in the dark for 24 h and then filtered. **BiBzIm** (14.04 mg, 0.06 mmol) was added to the filtrate. The mixture was stirred at room temperature for 12 h to give a yellow solution. **L** (20.76 mg, 0.06 mmol) and excess strontium hydroxide octahydrate (21.34 mg,

0.06mmol) was then added. The mixture was stirred at room temperature for another 12 h to give a yellow solution. The solvent was concentrated to about 3 mL. Upon the addition of diethyl ether, a yellow solid was precipitated and collected. The product was recrystallized from a CH_3OH/diethyl ether mixture to afford block-shaped crystals (**3**).

Characterization data for 3 (**Trefoil knot**): 73.42 mg, yield 82.3%. δ 8.60 (d, *J* = 5.6 Hz, 12H, pyridyl-αH), δ 7.14 (d, *J* = 5.6 Hz, 12H, pyridyl-αH), δ 8.15-8.12 (m, 12H, BiBzIm-H), δ 7.55-7.48 (m, 12H, BiBzIm-H), δ 3.58 (d, *J* = 15.2 Hz, 6H, phenyl-H), δ 1.64 (d, *J* = 15.2 Hz, 6H, phenyl-H), δ 1.73 (s, 90H, Cp*-H). IR (KBr disk, cm^{-1}): v = 1709, 1671, 1617, 1534, 1454, 1417, 1373, 1333, 1271, 1224, 1143, 1067, 1031, 1003, 963, 771, 638, 572, 445. Anal. Calcd for $C_{170}H_{170}O_{31}N_{24}S_8F_{24}SrRh_6$ (M = 4460.32): C, 45.75; H, 3.84; N, 7.53. Found: C, 45.73; H, 3.81, N, 7.55. ESI-MS: m/z 2072.21 (calcd for $[M - H_2O - 2OTf^-]^{2+}$ 2072.21).

Synthesis of 4 (**Trefoil knot**). $AgSO_3CF_3$ (62 mg, 0.24 mmol) was added to a solution of $[Cp^*RhCl_2]_2$ (37.2 mg, 0.06 mmol) in CH_3OH (6 mL) at room temperature. The reaction mixture was stirred in the dark for 24 h and then filtered. **BiBzIm** (14.04 mg, 0.06 mmol) was added to the filtrate. The mixture was stirred at room temperature for 12 h to give a yellow solution. **L** (20.76 mg, 0.06 mmol) and excess barium nitrate (15.68 mg, 0.06mmol) was then added. The mixture was stirred at room temperature for another 12 h to give a yellow solution. The solvent was concentrated to about 4 mL. Upon the addition of diethyl ether, a yellow solid was precipitated and collected. The product was recrystallized from a CH_3OH/diethyl ether mixture to afford block-shaped crystals (**4**).

Characterization data for 4: 86.86 mg, yield 84.0%. ^1H NMR (400 MHz, CD_3OD, ppm, with respect to Cp*Rh): δ 8.60 (d, *J* = 6.4 Hz, 12H, pyridyl-αH), δ 7.14 (d, *J* = 6.4 Hz, 12H, pyridyl-αH), δ 8.14-8.12 (m, 12H, BiBzIm-H), δ 7.52-7.48 (m, 12H, BiBzIm-H), δ 3.58 (d, *J* = 14.8 Hz, 6H, phenyl-H), δ 1.64 (d, *J* = 15.2 Hz, 6H, phenyl-H), δ 1.73 (s, 90H, Cp*-H). IR (KBr disk, cm^{-1}): v = 1709, 1671, 1617, 1534, 1454, 1417, 1373, 1333, 1271, 1224, 1143, 1067, 1031, 1003, 963, 771, 638, 572, 445. Anal. Calcd for $C_{178}H_{194}O_{43}N_{24}S_{11}F_{30}Ba_2Rh_6$ (M = 5170.26): C, 41.33; H, 3.78; N, 6.50. Found: C, 41.35; H, 3.80, N, 6.52.

3. Single-crystal X-ray structure of figure-eight knot, 1, 2, 3a, 4

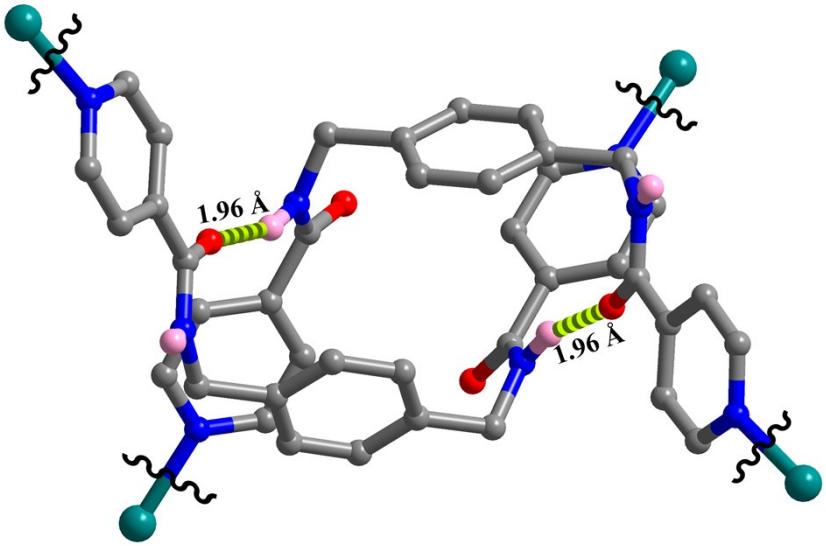

Fig. S1. Intramolecular hydrogen-bond interactions in crystallographically-derived structure of **figure-eight knot**

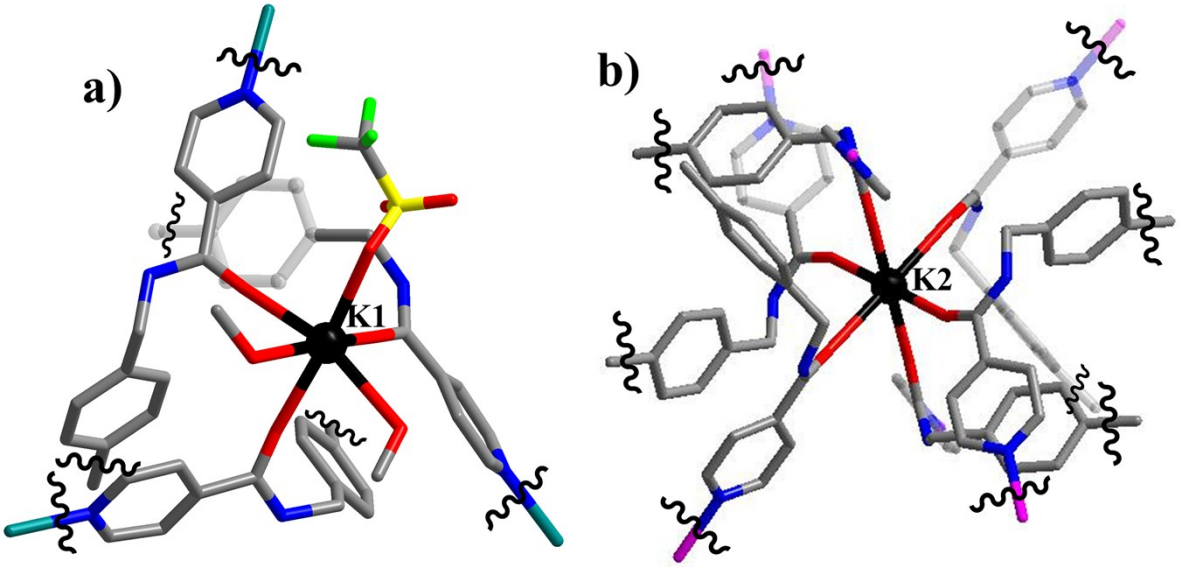

Fig. S2. a) Coordination-section of $K1^+$ cations showing that $K1^+$ cations are coordinated to three amide oxygens, two CH_3OH and one OTf^- anions; **b**) Coordination-section of $K2^+$ cations showing that $K2^+$ cations are coordinated to six amide oxygens. Other counteranions and hydrogen atoms are omitted for clarity (N, blue; C, grey; Rh, teal; K, black; O, red; F, bright green; S, yellow).

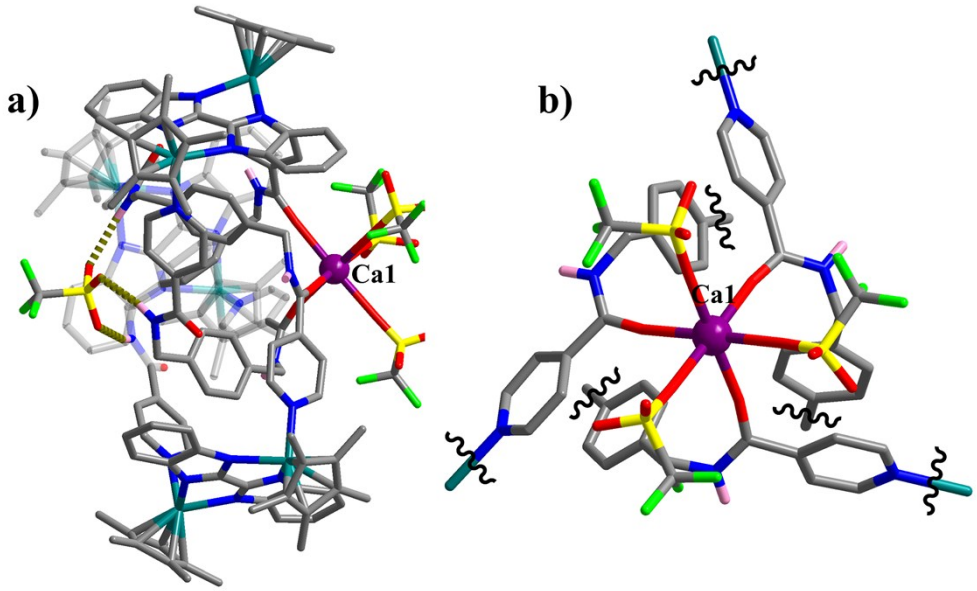

Fig. S3. a) Intermolecular hydrogen-bond interactions in crystallographically-derived structure of **2**; **b**) coordination-section of Ca^{2+} cations showing that Ca^{2+} cations are coordinated to three amide oxygens and three OTf- anions. Other counteranions and hydrogen atoms are omitted for clarity (N, blue; C, grey; Rh, Teal; Ca, Violet; H, rose; O, red; F, bright green; S, yellow).

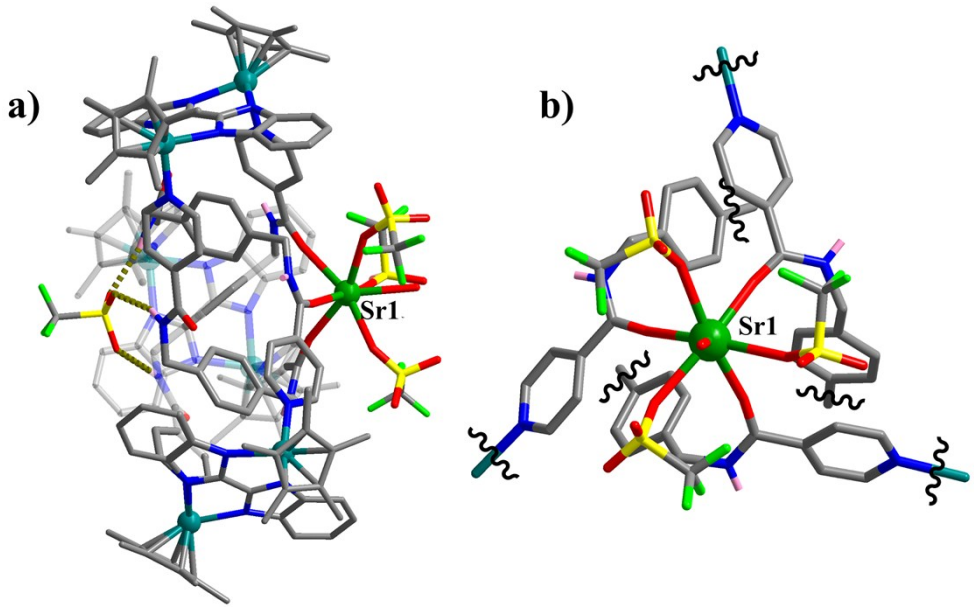

Fig. S4. a) Intermolecular hydrogen-bond interactions in crystallographically-derived structure of **3a**; **b**) coordination-section of Sr^{2+} cations showing that Sr^{2+} cations are coordinated to three amide oxygens, three OTf- anions and one H_2O molecule. Other counteranions and hydrogen atoms are omitted for clarity (N, blue; C, grey; Rh, Teal; Sr, Green; H, rose; O, red; F, bright green; S, yellow).

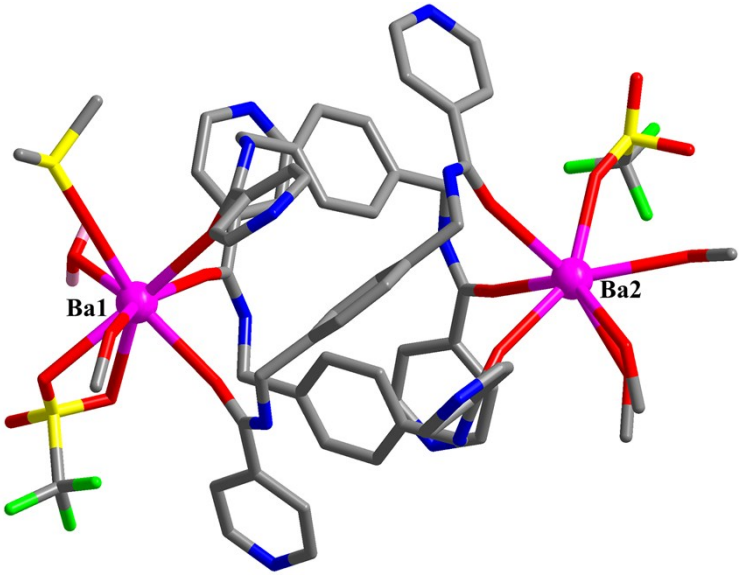

Fig. S5. Coordination-section of barium ions of complex **4** showing that $Ba1^{2+}$ cations are coordinated to one CH_3OH, DMSO, H_2O and OTf^- anion, $Ba2^{2+}$ cations are coordinated to three CH_3OH, one H_2O and OTf^- anion. Other counteranions and hydrogen atoms are omitted for clarity (N, blue; C, grey; Rh, Teal; Ba, Pink; H, rose; O, red; F, bright green; S, yellow).

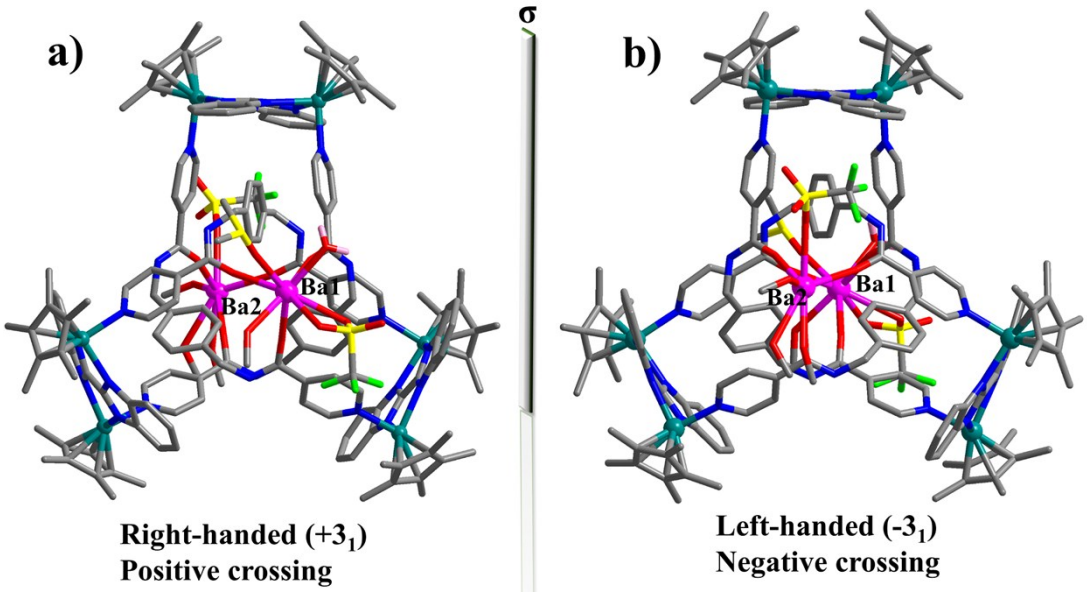

Fig. S6. Two mirror symmetric single-crystal X-ray structures of 4 (a, b).

4. NMR Spectra

4.1 NMR spectrum of 1

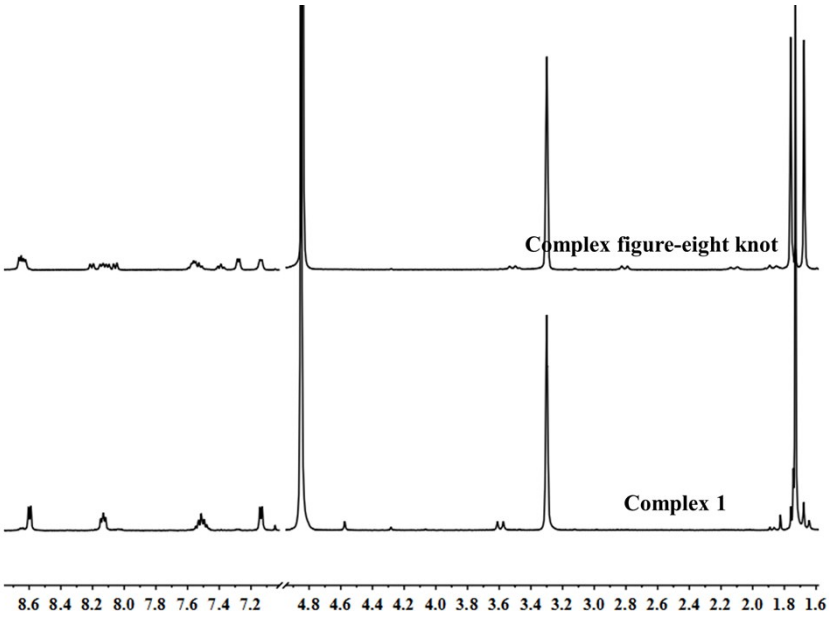

Fig. S7. ^{1}H NMR (400 MHz, CD_3OD, ppm) for complex **1** and figure-eight knot.

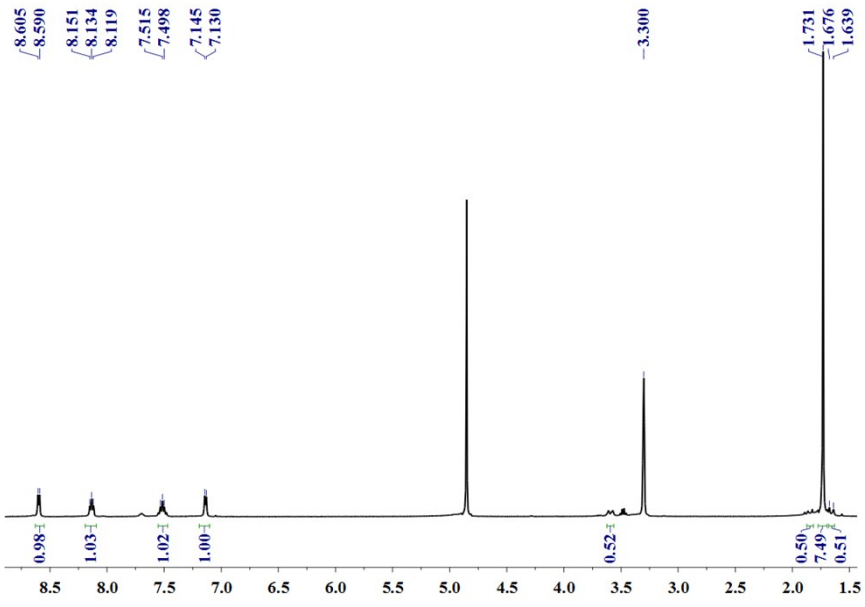

Fig. S8. ^{1}H NMR (400 MHz, CD_3OD, ppm) for complex **1** (20.0 mM, with respect to Cp*Rh).

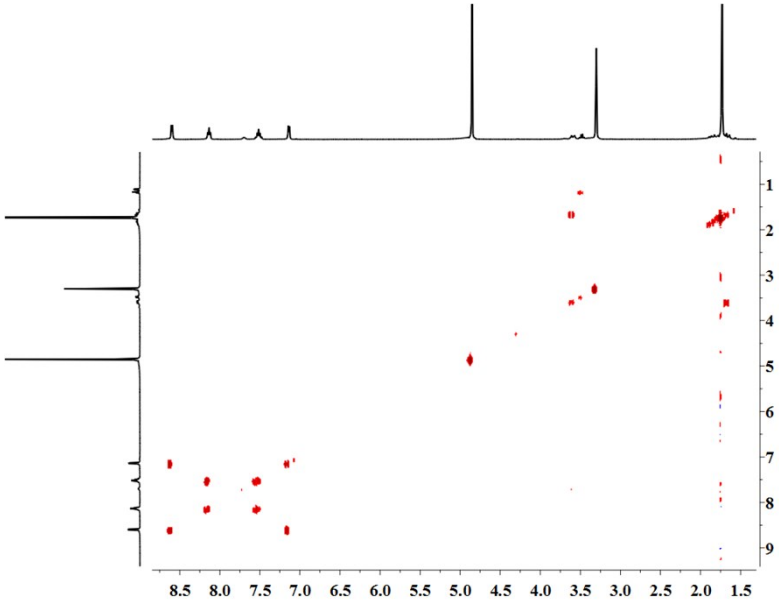

Fig. S9. ^{1}H COSY NMR (400 MHz, CD_3OD, ppm) for **1** (20.0 mM, with respect to Cp*Rh).

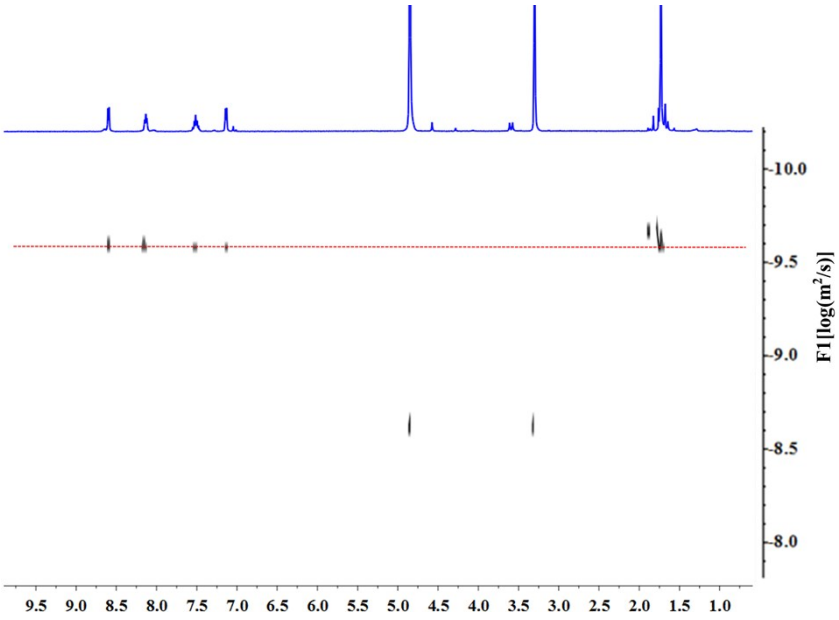

Fig. S10. ^{1}H DOSY NMR (400 MHz, CD_3OD, ppm) for **1** (23.0 mM, with respect to Cp*Rh) Diffusion coefficient: 2.6×10^{-10} m^2s^{-1}.

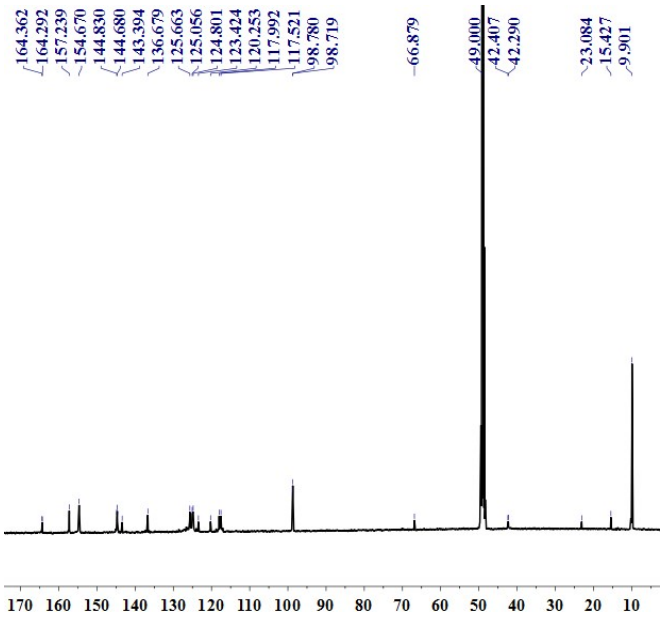

Fig. S11. $^{13}C\{^{1}H\}$ NMR (101 MHz, CD_3OD, ppm) for **1** (15.0 mM, with respect to Cp*Rh).

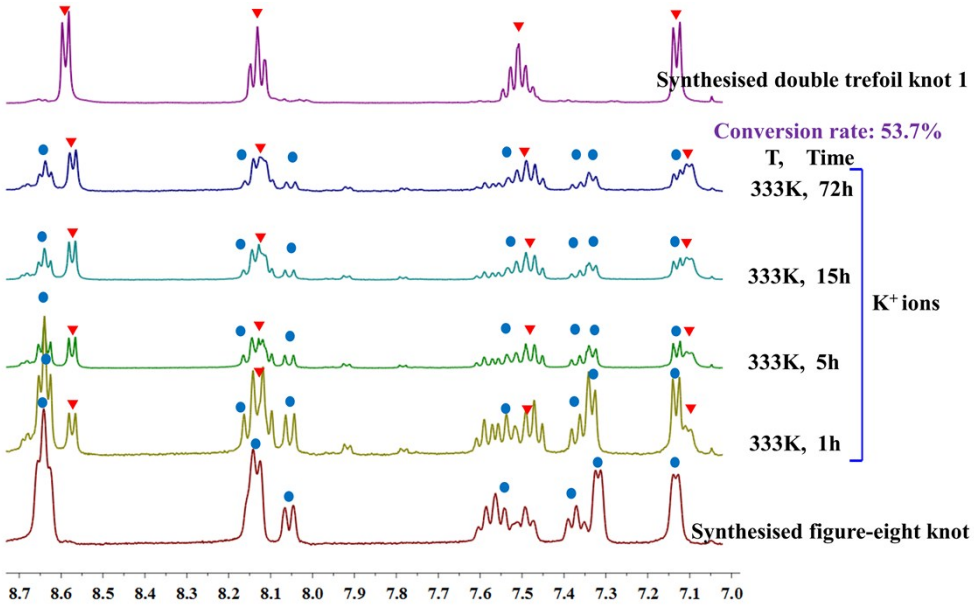

Fig. S12. Partial ^{1} H NMR spectra (CD_3OD, 400 MHz, 333 K) concerning structural unlinking transformation of figure-eight knot to double trefoil knot **1** induced by K^+ ions. Blue circles denote signals of figure-eight knot; red triangles denote double signals of the trefoil knots.

4.2 NMR spectrum of 2

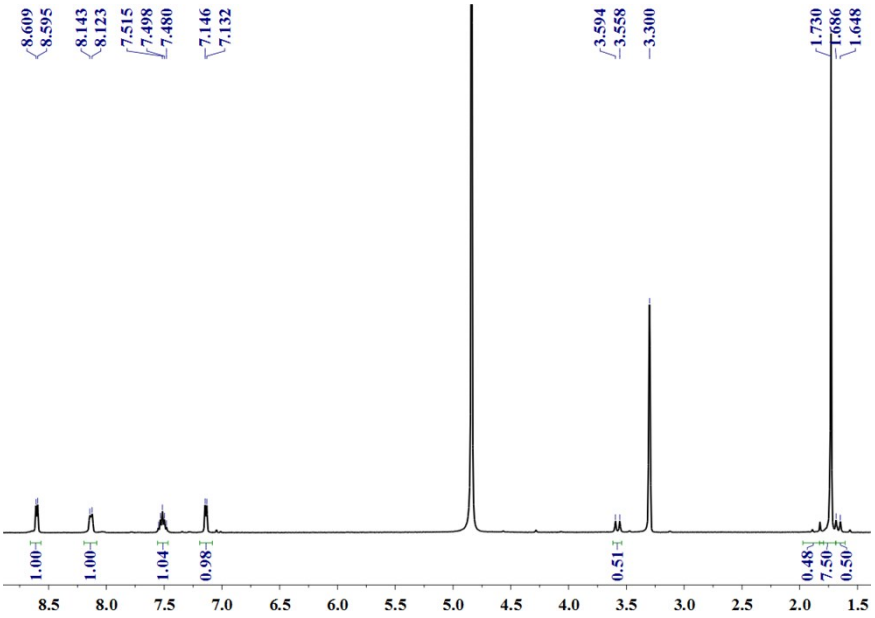

Fig. S13. ^{1}H NMR (400 MHz, CD_3OD, ppm) for complex **2** (25.0 mM, with respect to Cp*Rh).

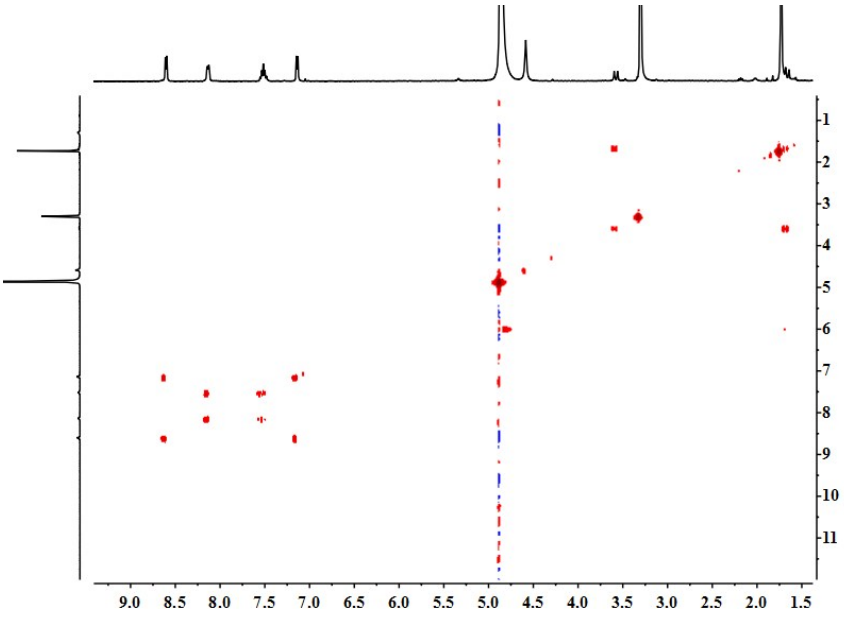

Fig. S14. ^{1}H COSY NMR (400 MHz, CD_3OD, ppm) for complex **2** (18.0 mM, with respect to Cp*Rh).

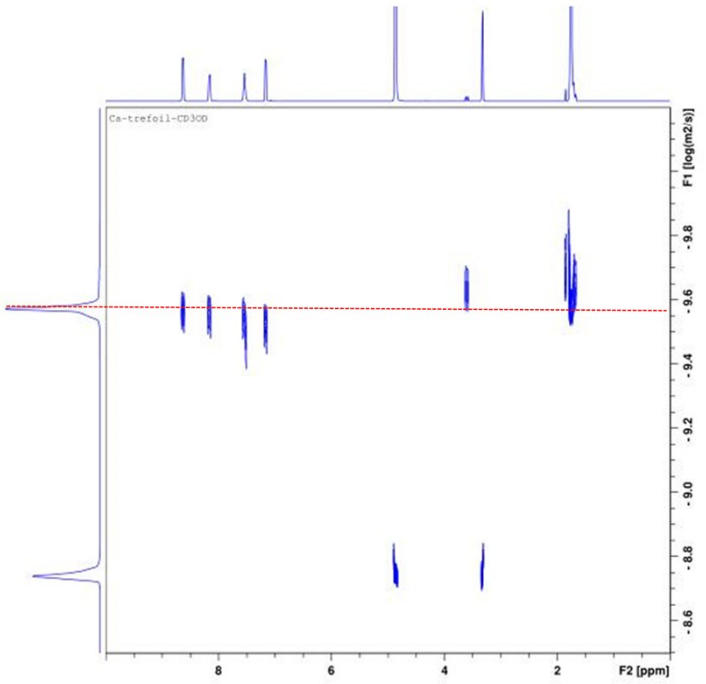

Fig. S15. ^{1}H DOSY NMR (400 MHz, CD_3OD, ppm) for **2** (15.0 mM, with respect to Cp*Rh) Diffusion coefficient: 2.7×10^{-10} m^2s^{-1}.

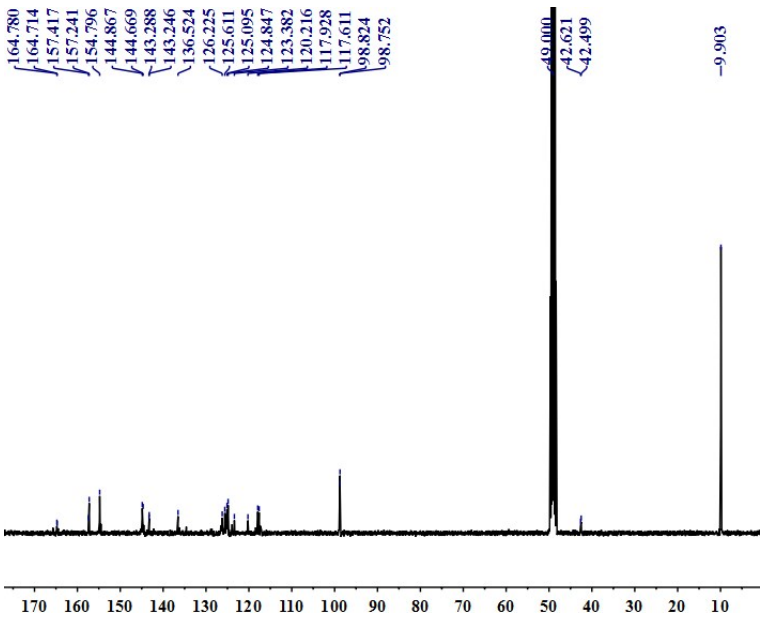

Fig. S16. $^{13}C\{^{1}H\}$ NMR (101 MHz, CD_3OD, ppm) for **2** (20.0 mM, with respect to Cp*Rh).

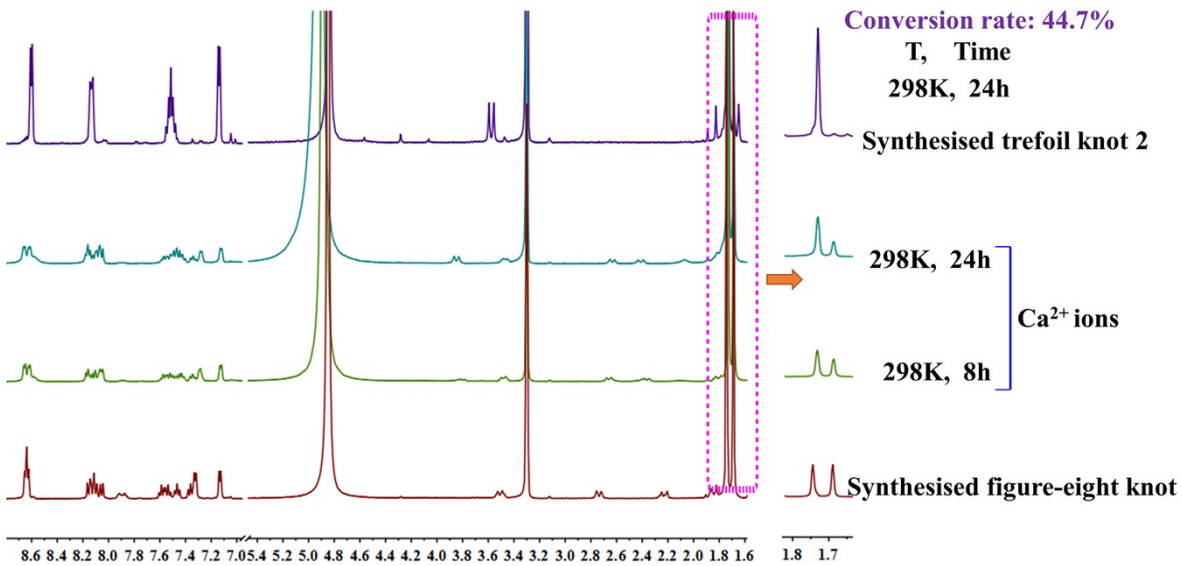

Fig. S17. ^{1}H NMR (400 MHz, CD_3OD, ppm) for **figure-eight knot+2** with increasing proportion of trefoil knot **2** upon addition of two equivalents of $Ca(NO_3)_2{\cdot}4H_2O$ (15.0 mM, with respect to Cp*Rh).

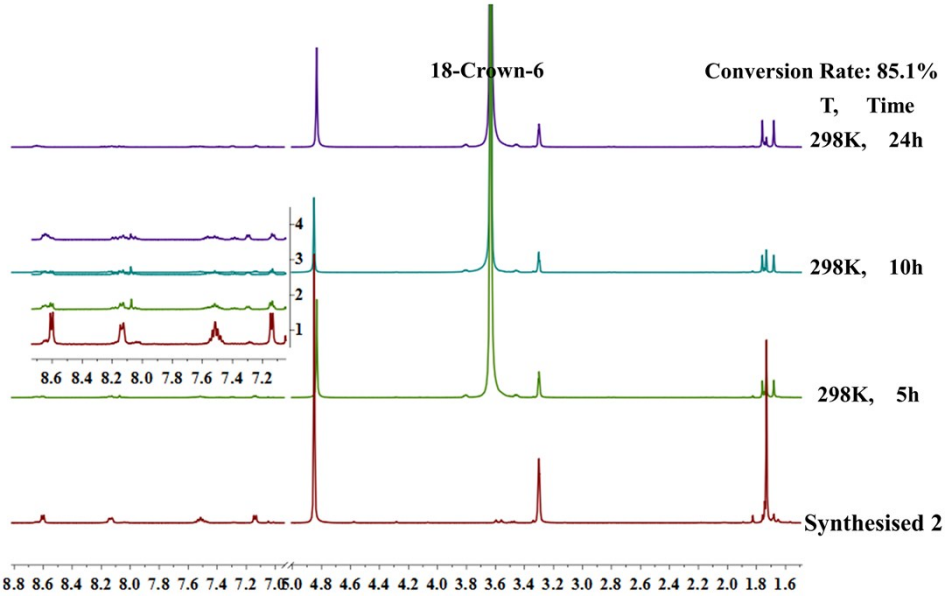

Fig. S18. ^{1}H NMR (400 MHz, CD_3OD, ppm) for **2+figure-eight knot** with increasing proportion of **figure-eight knot** upon addition of two equivalents of 18-crown-6 (18.0 mM, with respect to Cp*Rh).

4.3 NMR spectrum of 3

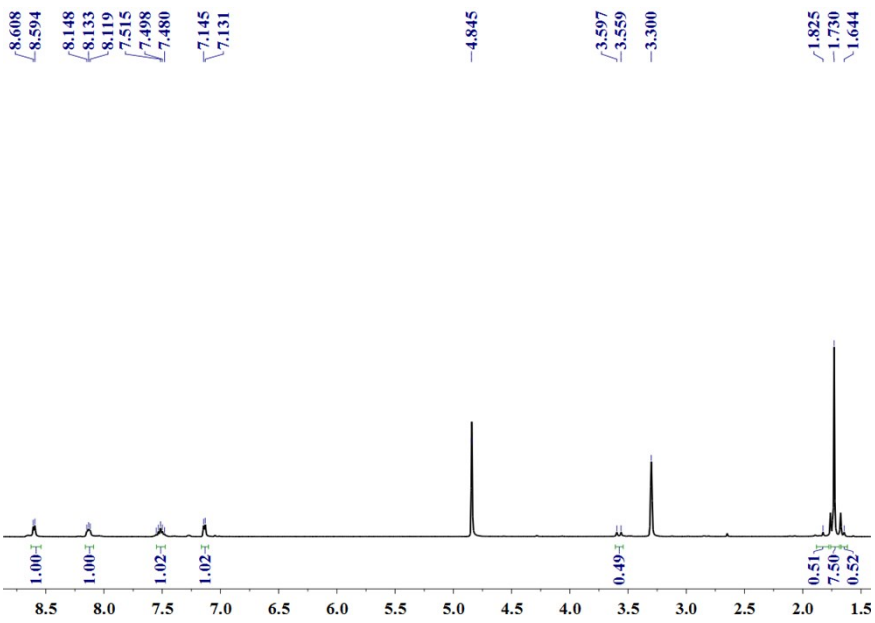

Fig. S19. ^{1}H NMR (400 MHz, CD_3OD, ppm) for complex **3** (20.0 mM, with respect to Cp*Rh).

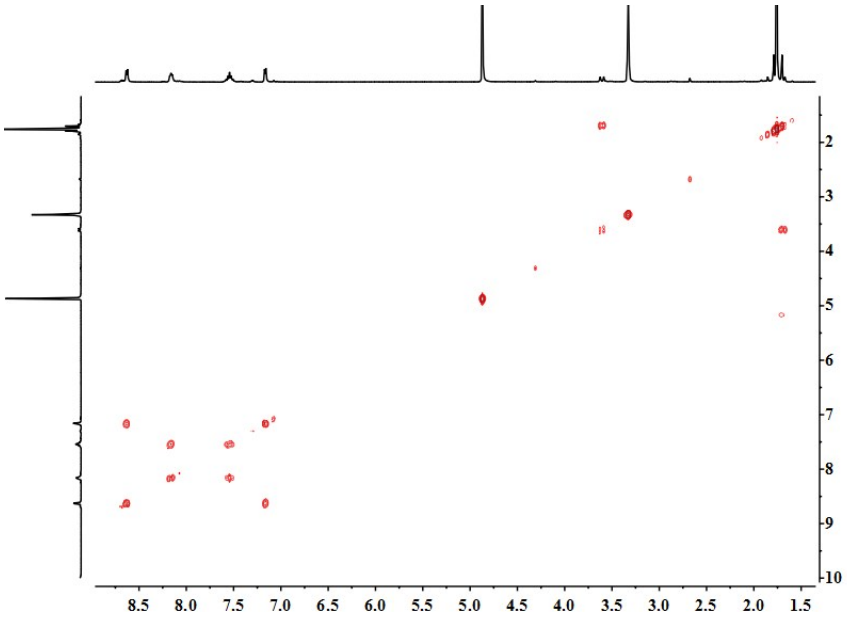

Fig. S20. ^{1}H COSY NMR (400 MHz, CD_3OD, ppm) for **3** (20.0 mM, with respect to Cp*Rh)

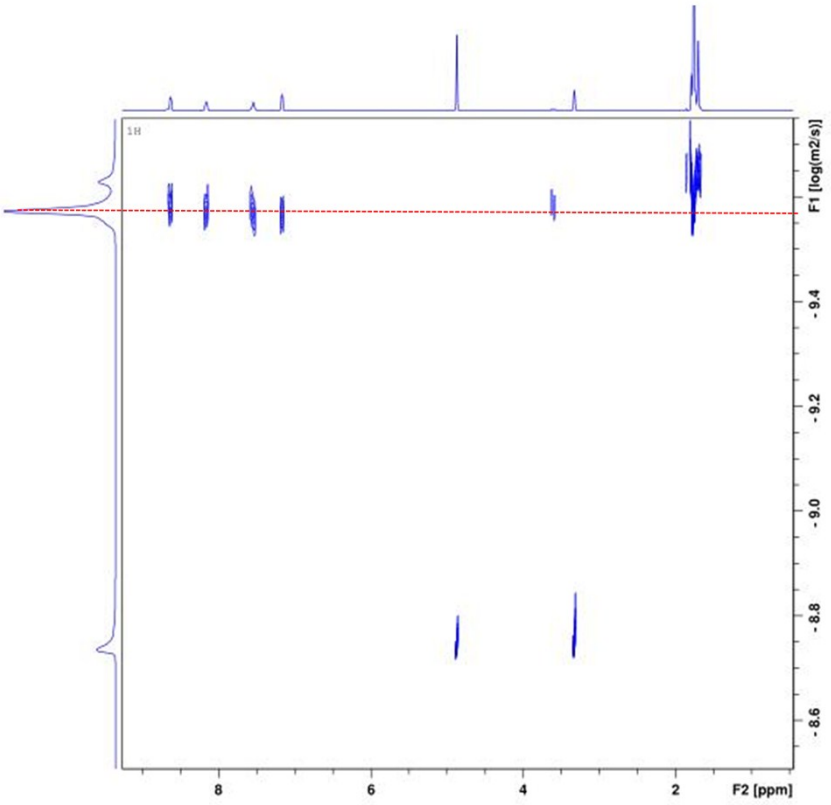

Fig. S21. ^{1}H DOSY NMR (400 MHz, CD_3OD, ppm) for **3** (20.0 mM, with respect to Cp*Rh) Diffusion coefficient: 2.7×10^{-10} m^2s^{-1}

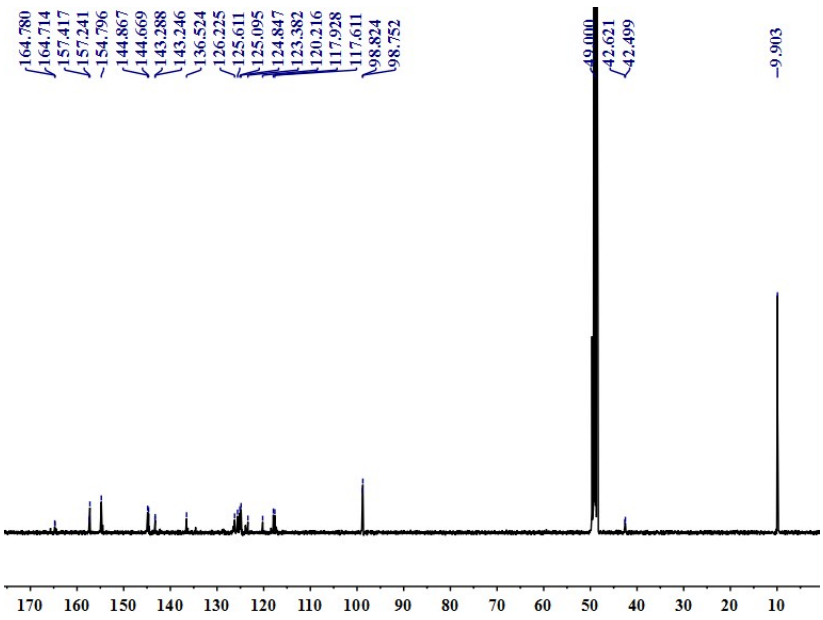

Fig. S22. $^{13}C\{^{1}H\}$ NMR (101 MHz, CD_3OD, ppm) for **3** (20.0 mM, with respect to Cp*Rh).

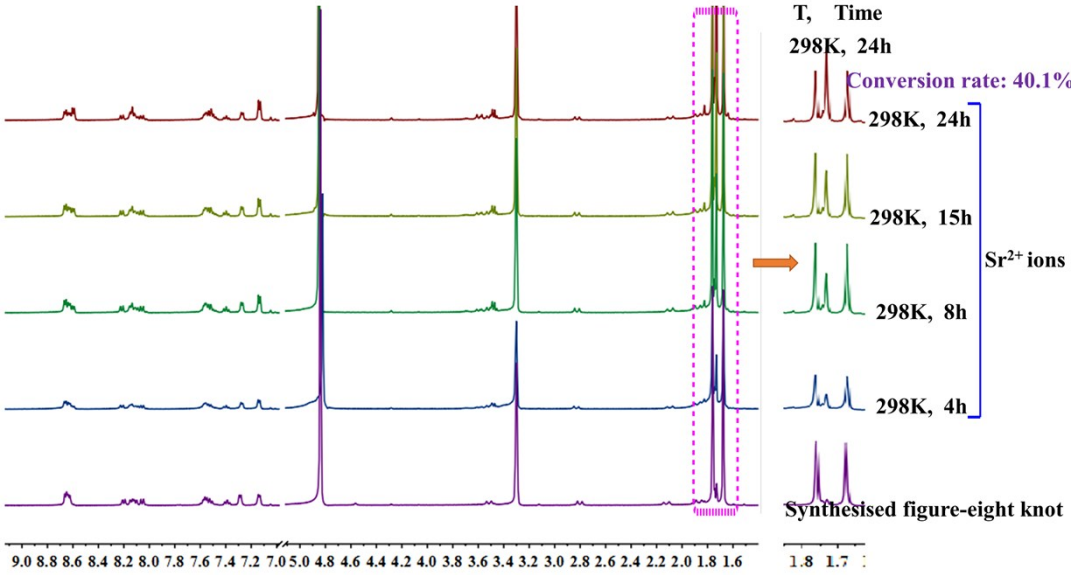

Fig. S23. ^{1}H NMR (400 MHz, CD_3OD, ppm) for **figure-eight knot+3** with increasing proportion of trefoil knot **3** upon addition of two equivalents of $Sr(NO_3)_2$ (20.0 mM, with respect to Cp*Rh).

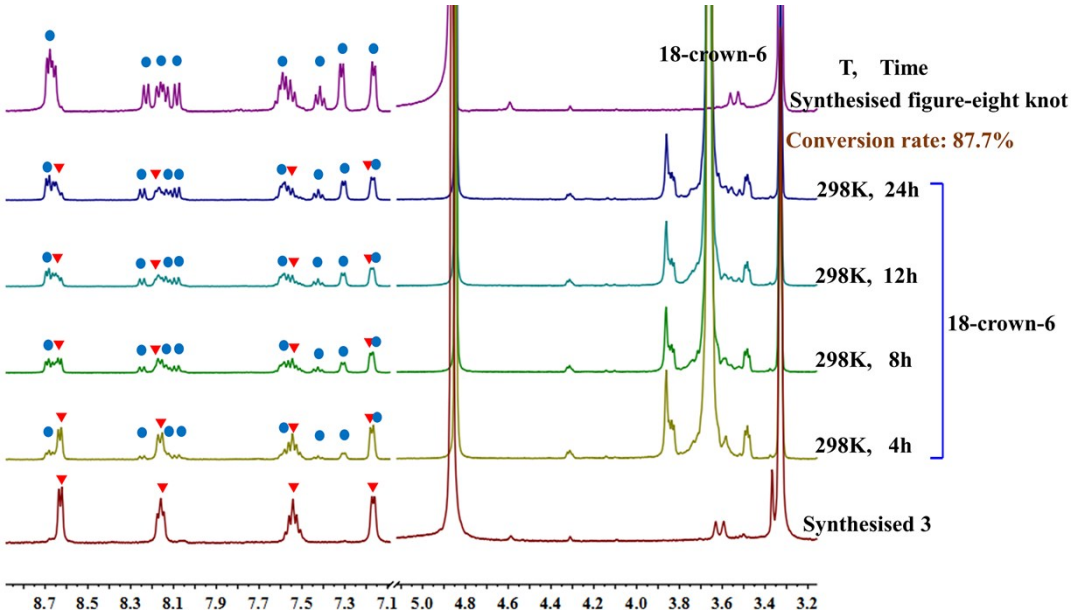

Fig. S24. ^{1}H NMR (400 MHz, CD_3OD, ppm) for **3+figure-eight knot** with increasing proportion of **figure-eight knot** upon addition of two equivalents of 18-crown-6 (20.0 mM, with respect to Cp*Rh).

4.4 NMR spectrum of 4

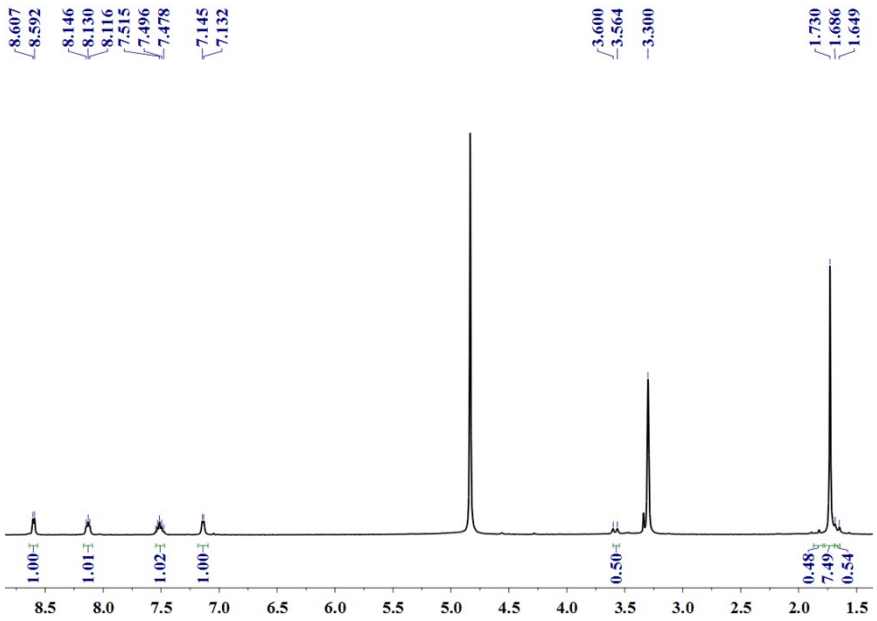

Fig. S25. [1] H NMR (400 MHz, CD_3OD, ppm) for **4** (15.0 mM, with respect to Cp*Rh).

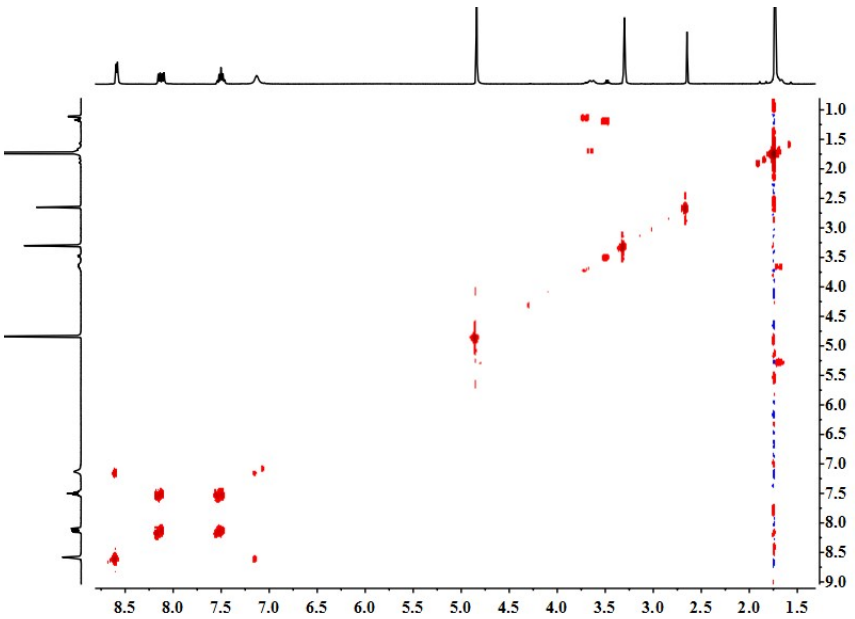

Fig. S26. [1]H COSY NMR (400 MHz, CD_3OD, ppm) for **4** (15.0 mM, with respect to Cp*Rh).

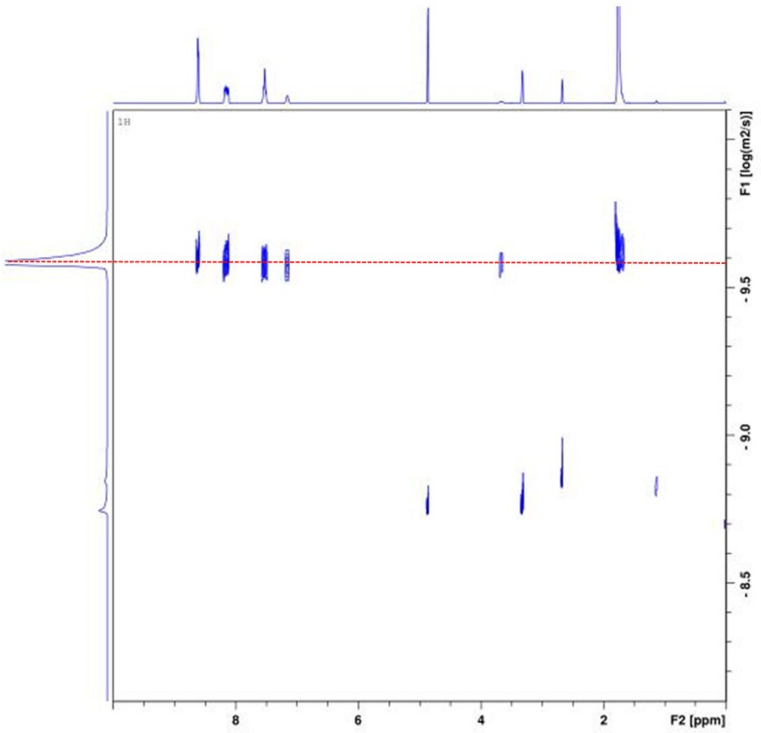

Fig. S27. ^{1}H DOSY NMR (400 MHz, CD_3OD, ppm) for **4** (15.0 mM, with respect to Cp*Rh) Diffusion coefficient: 2.4×10^{-10} m^2s^{-1}.

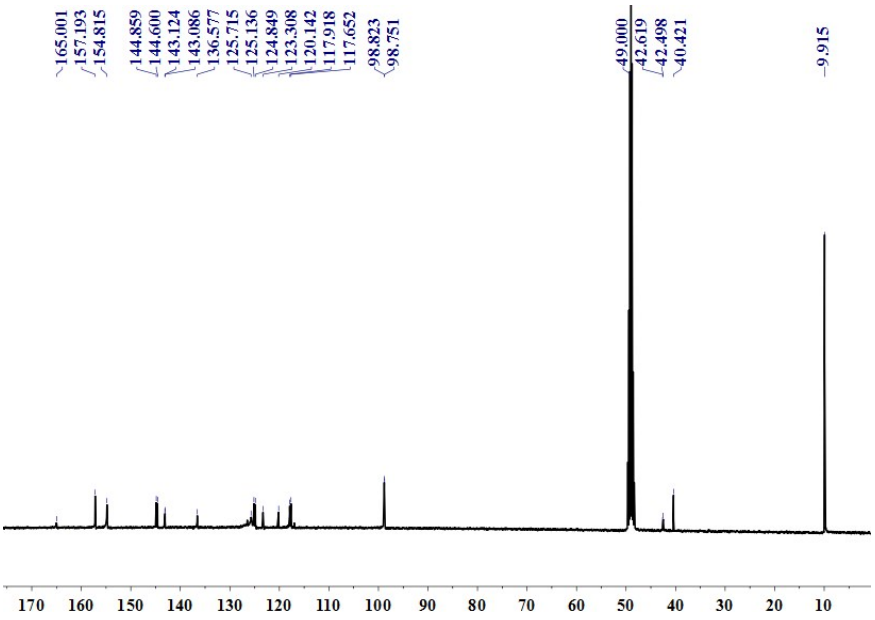

Fig. S28. $^{13}C\{^{1}H\}$ NMR (101 MHz, CD_3OD, ppm) for **4** (15.0 mM, with respect to Cp*Rh).

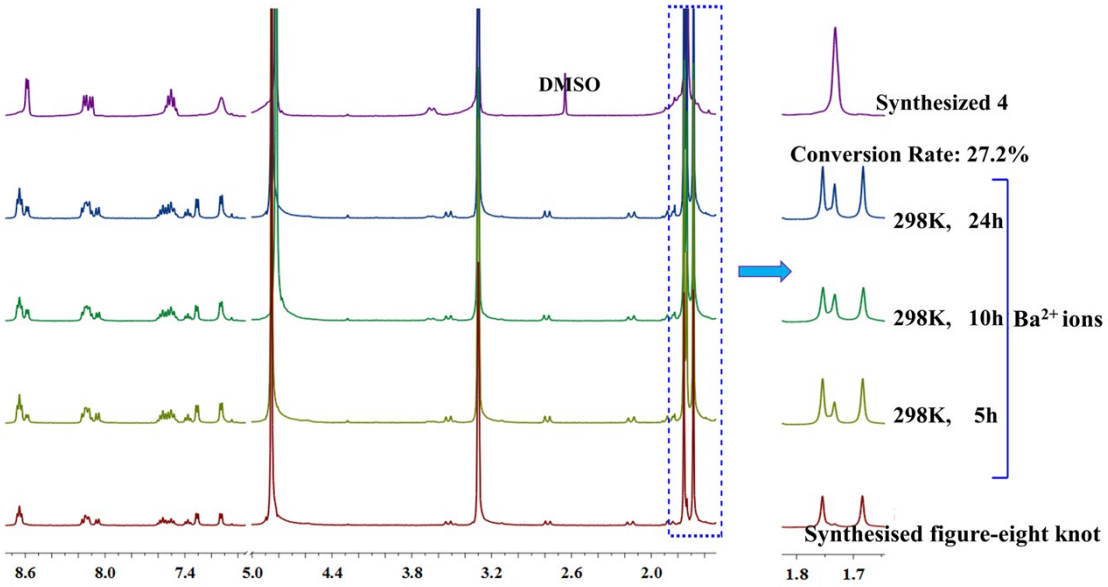

Fig. S29. [1] H NMR (400 MHz, CD_3OD, ppm) for **figure-eight knot+4** with increasing proportion of trefoil knot **4** upon addition of two equivalents of $Ba(NO_3)_2$ (15.0 mM, with respect to Cp*Rh).

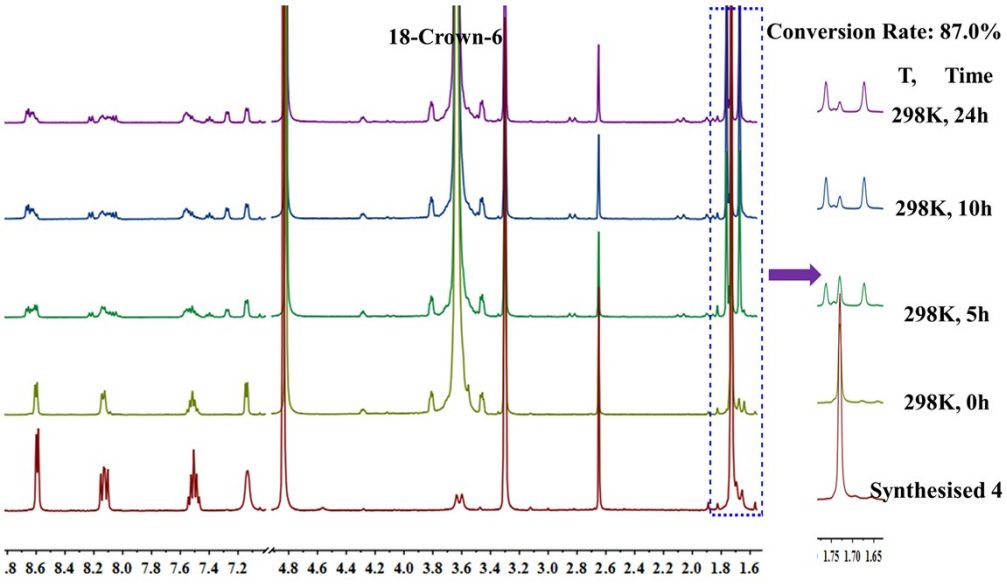

Fig. S30. [1]H NMR (400 MHz, CD_3OD, ppm) for **4+figure-eight knot** with increasing proportion of **figure-eight knot** upon addition of two equivalents of 18-crown-6 (15.0 mM, with respect to Cp*Rh).

5. ESI-MS spectra

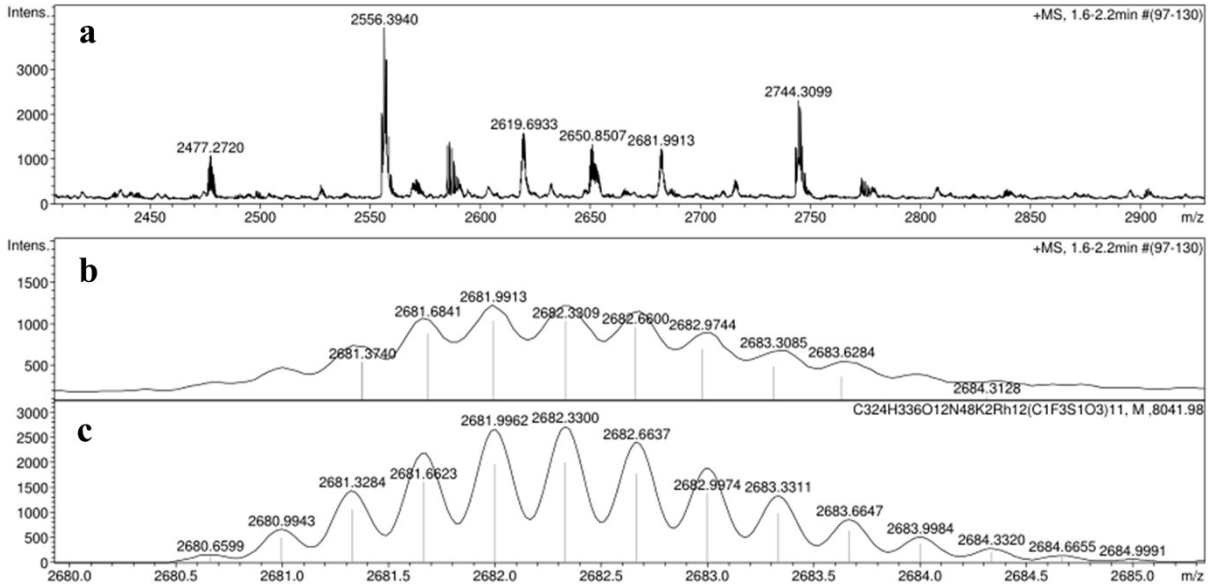

Fig. S31. Full ESI-MS spectra (**a**) of complex **1**, experimental (**b**) and theoretical (**c**) ESI-MS spectra of **[1 – 2CH_3OH–3OTf^-]$^{3+}$.**

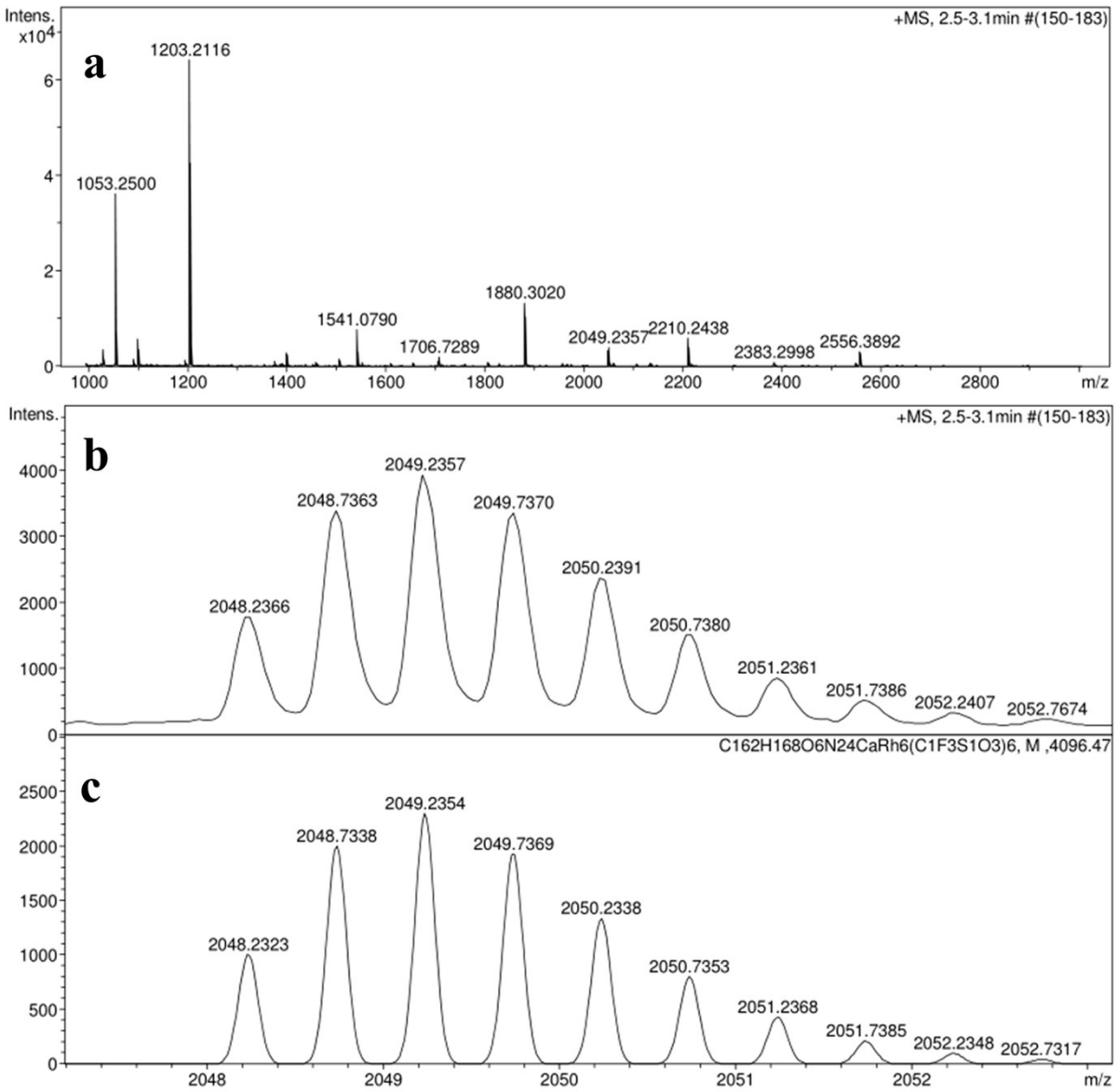

Fig. S32. Full ESI-MS spectra (**a**) of complex **2**, experimental (**b**) and theoretical (**c**) ESI-MS spectra of **[2 – 2OTf$^-$]$^{2+}$.**

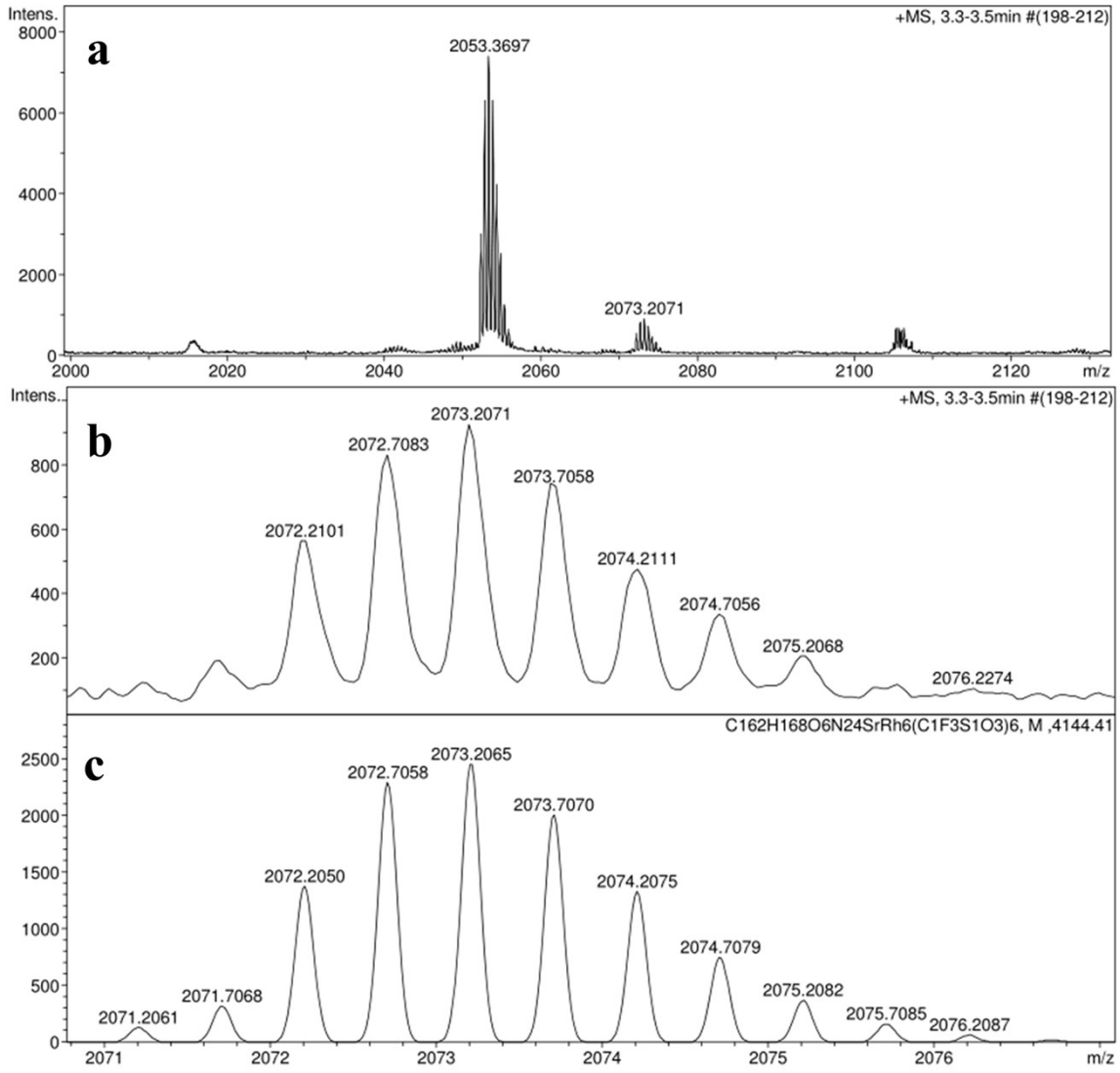

Fig. S33. Full ESI-MS spectra (**a**) of complex **3**, experimental (**b**) and theoretical (**c**) ESI-MS spectra of **[3 – H_2O–2OTf$^-$]$^{2+}$.**

6. DFT computational details.

The present first principle DFT calculations are performed by Vienna Ab initio Simulation Package (VASP) [4] with the projector augmented wave (PAW) method [5]. The exchange-functional is treated using the generalized gradient approximation (GGA) of Perdew-Burke-Ernzerhof (PBE) [6] functional. The cut-off energy of the plane-wave basis is set at 500 eV for optimize calculations of atoms and cell optimization. The Brillouin zone integration is performed using 3×3×1 Monkhorst-Pack [7] k-point sampling for a primitive cell. The self-consistent calculations apply a convergence energy threshold of 10-4eV. The equilibrium lattice constants are optimized with maximum stress on each atom within 0.05 eV/Å.

Table S1. Energetic results for the formation of a figure-eight knot from 4 ligands **L** and 4 building blocks **E** and for the formation of a trefoil knot from 3 ligands **L** and 3 building blocks **E**. Energy comparison (Same number of atoms): figure-eight knot × 3 = trefoil knot × 4.

Knot	Figure-eight knot	Trefoil
Total Energy/eV	-3145.85	-2357.99
Total Energy (Same number of atoms)/eV	-9437.55	-9431.96

Density functional theory (DFT) calculations shows that figure-eight knot has lower energy than trefoil knot in the absence of s-block metal ions.

Geometries:

All geometries presented here were optimized with long-range dispersion correction, i.e. using the PBE method.

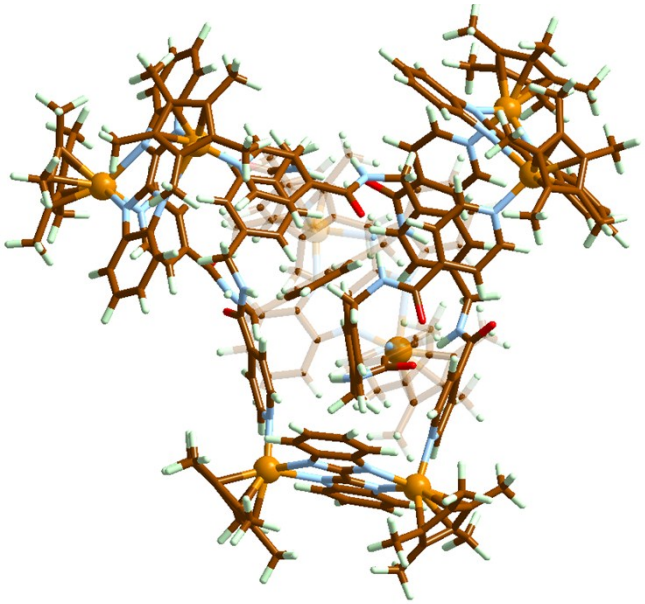

Fig. S34. Geometries of the figure-eight knot.

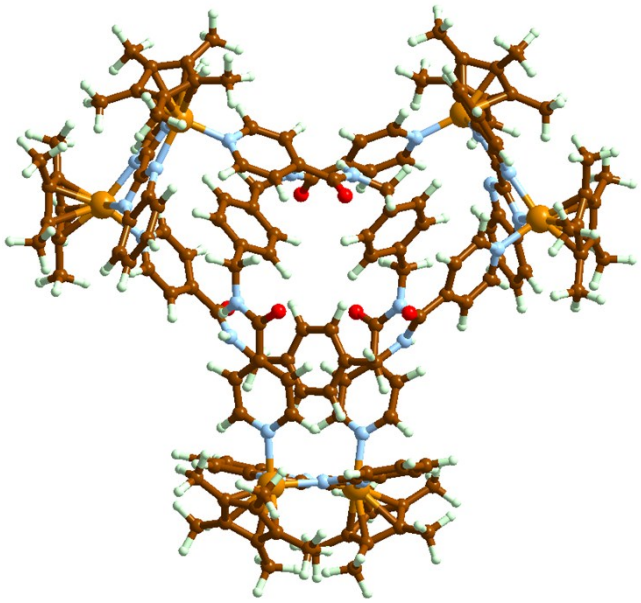

Fig. S35. Geometries of the trefoil knot.

7. X-ray crystallography details

Single crystals suitable for X-ray diffraction studies were obtained by recrystallization at room temperature. X-ray intensity data of **1**, **2**, **3a**, **3b** and **4** were collected on a CCD-Bruker SMART APEX diffractometer at 173 K. Disordered solvent molecules that could not be restrained properly were removed using the SQUEEZE routine in all data sets. Crystal data collection and refinement parameters of the X-ray diffraction studies are listed in Tables S2-S6. Single crystals of **1**, **2**, **3a**, **3b** and **4**, suitable for X-ray diffraction study were obtained at room temperature. X-ray intensity data of **1**, **2**, **3a**, **3b** and **4** were collected at 173 K on a CCD-Bruker SMART APEX system. In these data, the disordered solvent molecules which could not be restrained properly were removed using the SQUEEZE route.

In asymmetric unit of **2**, there were disordered anions and solvents (three triflate anions, five methanol and two water molecules) which could not be restrained properly. Therefore, SQUEEZE algorithm was used to omit them. 5 ISOR and 6 DFIX instructions were used to restrain anions and solvent molecule so that there were 25 restraints in the data. Hydrogen of some methanol and water molecules could not be found and others were put in calculated positions.

In asymmetric unit of **3a**, 3 ISOR and 4 DFIX instructions were used to restrain anions and Cp* fragments so that there were 23 restraints in the data. Hydrogen of water molecules could not be found and others were put in calculated positions.

In asymmetric unit of **3b**, there was one disordered water molecule which could not be restrained properly. Therefore, SQUEEZE algorithm was used to omit it. 3 ISOR and 4 DFIX instructions were used to restrain anions and solvent molecule so that there were 23 restraints in **3b**. Hydrogen of methanol and water molecules could not be found and others were put in calculated positions.

In asymmetric unit of **4**, there were disordered anions and solvents (four triflate anions, three dimethyl sulfoxide, five methanol and eight water molecules) which could not be restrained properly. Therefore, SQUEEZE algorithm was used to omit them. Two pentamethylcyclopentadienyl ligands (Cp* for short), three triflate anions, one DMSO and

one methanol molecules were disordered and they were divided into two parts (67:33 for Cp*, 63:37, 65:35, 75:25 for anions, 53:47 for DMSO and 58:42 for methanol). 124 ISOR, 6 SIMU, 2 DANG and 72 DFIX instructions were used to restrain anions, solvents and Cp* fragments so that there were 1070 restraints in the data. Hydrogen of some methanol and water molecules could not be found and others were put in calculated positions.

Table S2 Crystal data and structure refinement for 1

Empirical formula	$C_{340}H_{344}O_{56}N_{48}S_{14}F_{42}K_2Rh_{12}$	
Formula weight	8552.89	
Temperature/K	173.0	
Crystal system	triclinic	
Space group	P-1	
Unit cell dimensions	a/Å 22.5096(15)	α/° 72.977(3)
	b/Å 25.221(2)	β/° 89.886(4)
	c/Å 39.360(3)	γ/° 76.760(4)
Volume/Å^3	20748(3)	
Z	2	
ρcalcg/cm^3	1.511	
μ/mm^{-1}	3.467	
F(000)	9492.0	
Crystal size/mm^3	0.3 × 0.18 × 0.15	
Radiation	GaKα (λ = 1.34139)	
2Θ range for data collection/°	5.582 to 114	
Reflections collected	84738	
Independent reflections	84738 [R_{sigma} = 0.0555]	
Data/restraints/parameters	84738/17/4439	
Goodness-of-fit on F^2	2.124	
Final R indexes [I>=2σ (I)]	R_1 = 0.1885, wR_2 = 0.4726	
Final R indexes [all data]	R_1 = 0.2025, wR_2 = 0.4884	
Largest diff. peak/hole / e Å^{-3}	10.96/-2.38	

Table S3 Crystal data and structure refinement for 2

Empirical formula	$C_{170}H_{168}CaF_{24}N_{24}O_{30}Rh_6S_8$
Formula weight	4394.37
Temperature	173(2) K
Crystal system	hexagonal
Space group	$P6_3$
Unit cell dimensions	a = 23.302(5) Å α = 90.00(3)°
	b = 23.302(5) Å β = 90.00(3)°
	c = 21.347(4) Å γ = 120.00(3)°
Volume/Å^3	10039(5)
Z	2
ρ_{calc}g/cm^3	1.433
μ/mm^{-1}	3.684
F(000)	4398.0
Crystal size/mm^3	0.2 × 0.14 × 0.1
Radiation	GaKα (λ = 1.34138)
2Θ range for data collection/°	6.6 to 113.984
Index ranges	$-18 \le h \le 29$, $-28 \le k \le 28$, $-26 \le l \le 26$
Reflections collected	96191
Independent reflections	13702 [R_{int} = 0.0525, R_{sigma} = 0.0300]
Data/restraints/parameters	13702/98/761
Goodness-of-fit on F^2	1.068
Final R indexes [I>=2σ (I)]	R_1 = 0.0545, wR_2 = 0.1565
Final R indexes [all data]	R_1 = 0.0576, wR_2 = 0.1621
Largest diff. peak/hole / e Å^{-3}	0.76/-0.64

Table S4. Crystal data and structure refinement for 3a.

Empirical formula	$C_{170}\ H_{170}\ O_{31}\ N_{24}\ S_8\ F_{24}\ Sr\ Rh_6$	
Formula weight	4460.32	
Temperature	173(2) K	
Wavelength	1.34138 Å	
Crystal system	Hexagonal	
Space group	$P6_3$	
Unit cell dimensions	a = 22.673(5) Å	α/°= 90.00(3)°.
	b = 22.673(5) Å	β/°= 90.00(3)°.
	c = 20.482(4) Å	γ/°= 120.00(3)°.
Volume	9118(4) $Å^3$	
Z	2	
Density (calculated)	1.651 Mg/m^3	
Absorption coefficient	4.297 mm^{-1}	
F(000)	4602	
Crystal size	0.150 x 0.120 x 0.110 mm^3	
Theta range for data collection	3.392 to 54.940°.	
Index ranges	-23<=h<=27, -27<=k<=27, -24<=l<=24	
Reflections collected	76990	
Independent reflections	11512 [R(int) = 0.0921]	
Completeness to theta = 53.594°	99.7 %	
Absorption correction	Semi-empirical from equivalents	
Max. and min. transmission	0.751 and 0.551	
Refinement method	Full-matrix least-squares on F^2	
Data / restraints / parameters	11512 / 23 / 851	
Goodness-of-fit on F^2	1.053	
Final R indices [I>2sigma(I)]	R_1 = 0.0868, wR_2 = 0.1834	
R indices (all data)	R_1 = 0.1205, wR_2 = 0.2097	
Absolute structure parameter	0.18(3)	
Extinction coefficient	n/a	
Largest diff. peak and hole	1.710 and -0.853 $e.Å^{-3}$	

Table S5. Crystal data and structure refinement for 3b.

Empirical formula	$C_{173}\ H_{189}\ F_{24}\ N_{24}\ O_{37.50}\ Rh_6\ S_8\ Sr$
Formula weight	4622.03
Temperature	173(2) K
Wavelength	1.34138 Å
Crystal system	Hexagonal
Space group	$P6_3$
Unit cell dimensions	a = 22.564(3) Å □ α/°= 90°.
	b = 22.564(3) Å □ β/°= 90°.
	c = 20.375(3) Å □ γ/°= 120°.
Volume	8984(3) Å3
Z	2
Density (calculated)	1.709 Mg/m3
Absorption coefficient	4.378 mm-1
F(000)	4694
Crystal size	0.200 × 0.120 × 0.100 mm3
Theta range for data collection	3.408 to 55.450°.
Index ranges	-25<=h<=27, -27<=k<=25, -25<=l<=24
Reflections collected	74772
Independent reflections	11456 [R(int) = 0.0779]
Completeness to theta = 53.594°	99.7 %
Absorption correction	Semi-empirical from equivalents
Max. and min. transmission	0.734 and 0.557
Refinement method	Full-matrix least-squares on F2
Data / restraints / parameters	11456 / 23 / 825
Goodness-of-fit on F2	1.075
Final R indices [I>2sigma(I)]	R1 = 0.1065, wR2 = 0.3181
R indices (all data)	R1 = 0.1109, wR2 = 0.3222
Absolute structure parameter	0.22(4)
Extinction coefficient	n/a
Largest diff. peak and hole	2.627 and -1.385 e.Å-3

Table S6. Crystal data and structure refinement for 4.

Empirical formula	$C_{190}\ H_{252}\ Ba_2\ F_{30}\ N_{24}\ O_{60}\ Rh_6\ S_{14}$	
Formula weight	5743.12	
Temperature	173.05 K	
Wavelength	1.34138 Å	
Crystal system	Monoclinic	
Space group	C12/c1	
Unit cell dimensions	a = 72.911(5) Å	α/°= 90°.
	b = 20.9282(14) Å	β/°= 106.419(2)°.
	c = 33.246(2) Å	γ/° = 90°.
Volume	48661(6) $Å^3$	
Z	8	
Density (calculated)	1.568 Mg/m^3	
Absorption coefficient	5.125 mm^{-1}	
F(000)	23328	
Crystal size	0.02 x 0.02 x 0.01 mm^3	
Theta range for data collection	2.766 to 55.053°.	
Index ranges	-88<=h<=88, -23<=k<=25, -40<=l<=40	
Reflections collected	245168	
Independent reflections	46319 [R(int) = 0.0657]	
Completeness to theta = 53.594°	99.9 %	
Absorption correction	Semi-empirical from equivalents	
Max. and min. transmission	0.7508 and 0.5487	
Refinement method	Full-matrix least-squares on F^2	
Data / restraints / parameters	46319 / 1070 / 2061	
Goodness-of-fit on F^2	1.346	
Final R indices [I>2sigma(I)]	R1 = 0.0929, wR2 = 0.2998	
R indices (all data)	R1 = 0.1012, wR2 = 0.3130	
Extinction coefficient	n/a	
Largest diff. peak and hole	2.503 and -1.691 $e.Å^{-3}$	

[a] $R_1 = \Sigma||F_o| - |F_c||$ (based on reflections with $Fo^2 > 2\sigma F^2$); $wR_2 = \{\Sigma[\omega(Fo^2 - Fc^2)^2]/\Sigma[\omega(Fo^2)^2]\}^{1/2}$; $w = 1/[\sigma^2 F0^2 + (0.095P)^2]$; $P = [\max(Fo^2, 0) + 2Fc^2]/3$ (also with $Fo^2 > 2\sigma F^2$

9. References

1. C. White, A. Yates and P. M. Maitlis, η5 -Pentamethylcyclopentadienyl) rhodium and -iridium compounds. Inorg. Synth., 1992, **29**, 228–234.
2. T. Wu, L. H. Weng and G. X. Jin, Sunlight induced cycloaddition and host–guest property of self-assembled organometallic macrocycles based on a versatile building block. Chem. Comm., 2012, **48**, 4435–4437.
3. L. L. Dang, Z. B. Sun, W. L. Shan, Y. J. Lin, Z. H. Li, G. X. Jin, Coordination-driven self-assembly of a molecular figure-eight knot and other topologically complex architectures. Nat. Commun., 2019, **10**, 2057.
4. G. Kresse, D. Joubert, Phys. Rev. B 1999, 59, 1758.
5. J. P. Perdew, K. Burke, M. Ernzerhof, Phy. Rev. Lett. 1996, 77, 3865.
6. L. L. Gong, D. T. Zhang, C. Y. Lin, L. P Zhang and Z. H Xia, Adv. Energy Mater., 2019, 10.1002/aenm.201902625.
7. I. C. Man, H. Y. Su, F. Calle-Vallejo, H. A. Hansen, J. I. Martínez, N. G. Inoglu, J. Kitchin, T. F. Jaramillo, J. K. Nørskov, J. Rossmeisl, ChemCatChem, 2011, 3, 1159.

.